

Magnetic properties and magnetocaloric effects in $(Ho_{1-x}Y_x)_5Pd_2$ compounds

X F Wu(武小飞), C Guo(郭翠萍), G Cheng(成钢), C R Li(李长荣), J Wang(王江), Y S Du(杜玉松), G H Rao(饶光辉), Z Du(杜振民)

Citation: Chin. Phys. B . 2019, 28(5): 057502. **doi:** 10.1088/1674-1056/28/5/057502
Journal homepage: http://cpb.iphy.ac.cn; http://iopscience.iop.org/cpb

What follows is a list of articles you may be interested in

Ferromagnetism and magnetostructural coupling in V-doped MnNiGe alloys

Hui Yang(杨慧), Jun Liu(刘俊), Chao Li(李超), Guang-Long Wang(王广龙), Yuan-Yuan Gong(龚元元), Feng Xu(徐锋)
Chin. Phys. B . 2018, 27(10): 107502. **doi:** 10.1088/1674-1056/27/10/107502

Magnetostructural transformation and magnetocaloric effect in $Mn_{48-x}V_xNi_{42}Sn_{10}$ ferromagnetic shape memory alloys

Najam ul Hassan, Ishfaq Ahmad Shah, Tahira Khan, Jun Liu(刘俊), Yuanyuan Gong(龚元元), Xuefei Miao(缪雪飞), Feng Xu(徐锋)
Chin. Phys. B . 2018, 27(3): 037504. **doi:** 10.1088/1674-1056/27/3/037504

Magnetocaloric effect in the layered organic-inorganic hybrid $(CH_3NH_3)_2CuCl_4$

Yinina Ma(马怡妮娜), Kun Zhai(翟昆), Liqin Yan(闫丽琴), Yisheng Chai(柴一晟), Dashan Shang(尚大山), Young Sun(孙阳)
Chin. Phys. B . 2018, 27(2): 027501. **doi:** 10.1088/1674-1056/27/2/027501

Influences of P doping on magnetic phase transition and structure in MnCoSi ribbon

Du Qian-Heng, Chen Guo-Fu, Yang Wen-Yun, Hua Mu-Xin, Du Hong-Lin, Wang Chang-Sheng, Liu Shun-Quan, Han Jing-Zhi, Zhou Dong, Zhang Yan, Yang Jin-Bo
Chin. Phys. B . 2015, 24(6): 067502. **doi:** 10.1088/1674-1056/24/6/067502

Magnetic transition and large reversible magnetocaloric effect in $EuCu_{1.75}P_2$ compound

Huo De-Xuan, Liao Luo-Bing, Li Ling-Wei, Li Miao, Qian Zheng-Hong
Chin. Phys. B . 2013, 22(2): 027502. **doi:** 10.1088/1674-1056/22/2/027502

Magnetic properties and magnetocaloric effects in $(Ho_{1-x}Y_x)_5Pd_2$ compounds*

X F Wu(武小飞)[1,2,3], C P Guo(郭翠萍)[1,†], G Cheng(成钢)[2,3], C R Li(李长荣)[1], J Wang(王江)[2,3], Y S Du(杜玉松)[2,3,‡], G H Rao(饶光辉)[2,3], and Z M Du(杜振民)[1]

[1] *School of Materials Science and Engineering, University of Science and Technology Beijing, Beijing* 100083, *China*
[2] *School of Materials Science and Engineering, Guilin University of Electronic Technology, Guilin* 541004, *China*
[3] *Guangxi Key Laboratory of Information Materials, Guilin* 541004, *China*

(Received 26 December 2018; revised manuscript received 9 February 2019; published online 4 April 2019)

The crystal structure, magnetic and magnetocaloric properties of $(Ho_{1-x}Y_x)_5Pd_2$ ($x = 0$, 0.25, and 0.5) compounds are investigated. All the compounds crystallize in a cubic Dy_5Pd_2-type structure with the space group $Fd3m$ and undergo a second order transition from spin glass (SG) state to paramagnetic (PM) state. The spin glass transition temperatures T_g decrease from 26 K for $x = 0$ to 13 K for $x = 0.5$. In the PM region, the reciprocal susceptibilities for all the compounds obey the Curie–Weiss law. The paramagnetic Curie temperatures (θ_p) for Ho_5Pd_2, $(Ho_{0.75}Y_{0.25})_5Pd_2$, and $(Ho_{0.5}Y_{0.5})_5Pd_2$ are determined to be 32 K, 30 K, and 22 K, respectively, and the corresponding effective magnetic moments (μ_{eff}) are 10.8 μ_B/Ho, 10.3 μ_B/RE, and 7.5 μ_B/RE, respectively. Magnetocaloric effect (MCE) is anticipated according to the Maxwell relation, based on the isothermal magnetization curves. For a magnetic field change of 0–5 T, the maximum values of the isothermal magnetic entropy change $-\Delta S_M$ of the $(Ho_{1-x}Y_x)_5Pd_2$ ($x = 0$, 0.25, and 0.5) compounds are determined to be 11.5 J·kg^{-1}·K^{-1}, 11.1 J·kg^{-1}·K^{-1}, and 8.9 K J·kg^{-1}·K^{-1}, with corresponding refrigerant capacity values of 382.3 J·kg^{-1}, 336.2 J·kg^{-1}, and 242.5 J·kg^{-1}, respectively.

Keywords: $(Ho_{1-x}Y_x)_5Pd_2$ compounds, magnetic transition, magnetocaloric effect

PACS: 71.20.Eh, 75.30.Kz, 75.30.Sg **DOI:** 10.1088/1674-1056/28/5/057502

1. Introduction

The magnetocaloric effect (MCE) is an intrinsic thermal response of all magnetic materials. The magnetic refrigeration based on MCE is a promising alternative technology to the conventional gas compression or expansion refrigeration because of its higher energy efficiency and it is more friendly to the environmental.[1–5] MCE can be characterized by the isothermal magnetic entropy change (ΔS_M) or an adiabatic temperature change (ΔT_{ad}) when applying or removing a magnetic field. Another important parameter is the refrigerant capacity (RC), which is a measure of how much heat can be transferred between the cold and the hot sinks in one ideal refrigeration cycle, which depends on not only the ΔS_M but also the width of the ΔS_M–T curve.[2,6] According to the nature of the phase transition, the MCE materials can be divided into two kinds: first-order transition (FOT) and second-order transition (SOT) materials. FOT materials usually have large values of ΔS_M due to the abrupt change but are accompanied with remarkable thermal and magnetic hystereses, which reduce the effective RC values of magnetic materials.[7,8] In contrast, the ΔS_M of the SOT materials are generally smaller than those of the FOT materials but the SOT materials show a good reversible behavior of the magnetization in response to the temperature and magnetic fields. The success of the magnetic refrigeration technology depends substantially on the discovery of new materials with large MCE at the temperature of interest. Consequently, considerable efforts have been made to explore and develop new MCE materials in view of their applications in room temperature refrigeration to reduce the emission of green house gases. Several families of MCE materials with large MCE have been found, such as $Gd_5Si_{4-x}Ge_x$,[9,10] $La(Fe, Si)_{13}$,[11–14] $MnFeP_xAs_{1-x}$,[15] $MnAs_{1-x}Sb_x$,[16] and Heulser alloys Ni–Mn–X with (X = Ga, Sn, ...).[17–21] Meanwhile, the materials working at the low temperature regime are important because of their potential applications in special technological areas, such as space science, liquefaction of hydrogen in the fuel industry, and liquefaction of helium.[22] For this purpose, the rare earth (RE) based alloys and compounds have been systematically studied due to their magnetic transitions at low temperatures. Some have been found to possess excellent magnetocaloric properties,[23–46] such as $ErCo_2$, HoPd, TmGa, TmCuAl, HoFeSi, ErFeSi, Dy_3Al_2, Nd_7Pd_3, etc.

The binary RE–transition metal compounds of the type RE_5Pd_2 (RE = Tb, Dy, Ho) were first reported by Berkowitz

*Project supported by the National Basic Research Program of China (Grant No. 2014CB643703), the National Key Research and Development Program of China (Grant No. 2016YFB0700901), the National Natural Science Foundation of China (Grant Nos. 51261004 and 51761007), and Guangxi Natural Science Foundation, China (Grant No. 2018GXNSFAA294051).

†Corresponding author. E-mail: cpguo@ustb.edu.cn
‡Corresponding author. E-mail: duyusong@guet.edu.cn

© 2019 Chinese Physical Society and IOP Publishing Ltd

et al.[47] Loebich and Raub[48] then revealed the existence of Y_5Pd_2 and Er_5Pd_2 compounds. Fornasini and Palenzona investigated the crystal structure of the RE_5Pd_2 type compounds, and determined that all of them crystallized in a cubic Dy_5Pd_2-type structure (space group $Fd3m$).[49] Preliminary magnetic measurements of the RE_5Pd_2 compounds were carried out by Yakinthos *et al.*[50] They found that these compounds showed an antiferromagnetic transition with Néel temperatures between 15.0 K (Er) and 63.5 K (Tb). However, later investigations have suggested that RE_5Pd_2 owned a complex magnetic state. Klimczak *et al.* reported that the compounds RE_5Pd_2 (Tb-Er) ordered magnetically and showed a spin reorientation behavior;[51] while with the aid of dc and ac magnetic susceptibilities, magnetic memory effect, and heat capacity measurements, Sharma *et al.* proved that the Er_5Pd_2 compound underwent a spin-glass magnetic phase transition below 17.2 K, accompanied by a large magnetocaloric effect.[52] Very recently, a large change in the magnetic entropy was reported for the Dy_5Pd_2 compound and there was a magnetic glass behavior below 38 K.[53] By means of the neutron diffraction technique, the existence of the spin-glass behaviors in Ho_5Pd_2 and Tb_5Pd_2 below the spin-glass transition temperature T_g was confirmed[54] and a considerable value of relative cooling power (RCP) in the Ho_5Pd_2 compound have been observed.[55]

In the present work, we chose Ho_5Pd_2 as the matrix phase. The crystal structure, magnetic properties, and magnetocaloric behavior of Ho_5Pd_2, as well as the Y-doped compounds $(Ho_{1-x}Y_x)_5Pd_2$ ($x = 0.25$ and 0.5) have been studied in detail. The results show that all these compounds exhibit the spin-glass state and the T_g of $(Ho_{1-x}Y_x)_5Pd_2$ ($x = 0$, 0.25, and 0.5) is lowered with the increase of the yttrium content. The considerable magnetocaloric effects indicate that the series of the $(Ho_{1-x}Y_x)_5Pd_2$ compounds may be used for magnetic refrigeration application at low temperature.

2. Experimental details

Polycrystalline samples of $(Ho_{1-x}Y_x)_5Pd_2$ were prepared by an arc melting method under an argon atmosphere. The high purity Pd (99.95 wt.%), Ho (99.99 wt.%), and Y (99.99 wt.%) were re-melted more than four times to ensure homogeneity on a water-cooled copper hearth. To compensate the loss of Ho and Y during melting, 0.5% excess of Ho and 1% excess of Y were added and the total weight loss of the arc-cast sample was less than 0.5%. Subsequently, the alloy was sealed in an evacuated quartz tube and annealed at 800 K for 60 days and then quenched in ice-water mixture. Each sample was cut into two parts: the first was ground into powder for x-ray diffraction (XRD) analysis, which was carried out on a PANalytical PIXcel 3D x-ray powder diffractometer using Cu-$K\alpha_1$ radiation at 45 kV and 40 mA between 20° and 90°; the second was used for magnetic measurements. The phase and crystal structure were checked by Rietveld refinement of the XRD using the FullProf software. The temperature and magnetic field dependences of magnetizations were acquired on a commercial vibrating sample magnetometer (VSM) of the physical properties measurement system (PPMS-9, Quantum Design).

3. Results and discussion

Figure 1 shows the observed and refined powder XRD patterns of $(Ho_{1-x}Y_x)_5Pd_2$ ($x = 0$, 0.25, and 0.5) at room temperature (RT). The good match ($R_{wp} = 8.9\%$, $R_{exp} = 7.75\%$, $\chi^2 = 1.32$ for $x = 0$; $R_{wp} = 10.2\%$, $R_{exp} = 6.41\%$, $\chi^2 = 2.53$ for $x = 0.25$; $R_{wp} = 9.7\%$, $R_{exp} = 7.64\%$, $\chi^2 = 1.61$ for $x = 0.5$) between the observed and refined values indicates that all the compounds are single phase and crystallize in a cubic Dy_5Pd_2-type structure with the space group $Fd3m$. For comparison, the enlarged main characteristic diffraction peaks for the $(Ho_{1-x}Y_x)_5Pd_2$ ($x = 0$, 0.25, and 0.5) compounds are presented in the inset. We can clearly see that the positions of the diffraction peaks shift to a smaller angle when increasing the Y content, which should be related to the relative larger radius of the yttrium atom than that of holmium. The lattice parameter a and unit-cell volume V of the compound Ho_5Pd_2 are confirmed to be 13.4428 Å and 2429.2 Å^3, which are consistent with the previous reported data in Ref. [56]. The corresponding a and V for the $(Ho_{0.75}Y0_{.25})_5Pd_2$ and $(Ho_{0.5}Y_{0.5})_5Pd_2$ compounds are refined to be 13.4906 Å, 2455.2 Å^3 and 13.5315 Å, 2477.7 Å^3, respectively.

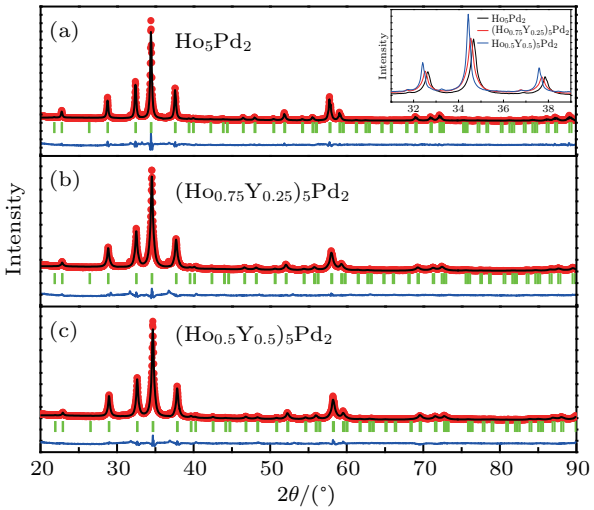


Fig. 1. The observed (dots) and calculated intensities (line drawn through the data points) of the fully refined powder diffraction pattern of (a) Ho_5Pd_2, (b) $(Ho_{0.75}Y_{0.25})_5Pd_2$, and (c) $(Ho_{0.5}Y_{0.5})_5Pd_2$. The short vertical lines indicate the calculated Bragg peak positions of the cubic Dy_5Pd_2-type crystal structure. The curve at the bottom of the plot shows the difference between the observed and calculated intensities. The inset shows the enlarged main characteristic diffraction peaks for the $(Ho_{1-x}Y_x)_5Pd_2$ ($x = 0$, 0.25, and 0.5) compounds.

The zero-field-cooled (ZFC) and field-cooled (FC) magnetization curves were measured under a magnetic field of 0.02 T for the $(Ho_{1-x}Y_x)_5Pd_2$ ($x = 0$, 0.25, and 0.5) compounds and the results are shown in Figs. 2(a)–2(c) (left scale), respectively. As can be seen, the ZFC curves for these compounds all show a cusp corresponding to the peak temperatures of 26 K, 20 K, and 13 K, respectively, indicating the presence of a magnetic phase transition. Additionally, the FC curves also show small peaks at the same temperatures with the ZFC curves, however, followed by an upturn. In general, a peak in the FC curve is observed in the systems that undergo an antiferromagnetic transition, while a small peak at glass transition temperature followed by a plateau has been reported in the spin-glass system.[57] The upturns in the FC curves below the magnetic transition temperature indicate the presence of clusters of spins.[58] Moreover, the spin-glass behavior in Ho_5Pd_2 below the magnetic phase transition temperature was also confirmed by the neutron diffraction technique, which is regarded as the most direct technology to determine the magnetic structure. Therefore, we can conclude that all the $(Ho_{1-x}Y_x)_5Pd_2$ ($x = 0$, 0.25, and 0.5) compounds undergo a spin-glass state to paramagnetic state magnetic transition at the T_g of 26 K, 20 K, and 13 K, respectively, and the temperature of spin-glass transition decreases with increasing yttrium content. Figure 2(a) (right-hand scale) shows the temperature dependence of the magnetic reciprocal susceptibility $1/\chi$ derived from the FC curve under a magnetic field of 200 Oe for Ho_5Pd_2. It is observed that the reciprocal susceptibility obeys Curie–Weiss law $\chi^{-1} = (T - \theta_p)/C$ in the PM region. Here θ_p is the paramagnetic Curie temperature and C is the Curie–Weiss constant. The effective magnetic moment derived from the Curie–Weiss constant is 10.8 μ_B/Ho atom, which is slightly higher than the theoretical value of Ho^{3+} (10.6 μ_B). It suggests that the Pd atom in the cubic structure Ho_5Pd_2 compound is non-magnetic. The value of the paramagnetic Curie temperature θ_p is determined to be 32 K, which is in agreement with the previous reported value of 33 K.[47] The positive value of θ_p indicates the dominance of ferromagnetic interactions in the spin-glass state. The temperature dependence of the magnetic reciprocal susceptibility for $(Ho_{0.75}Y_{0.25})_5Pd_2$ and $(Ho_{0.5}Y_{0.5})_5Pd_2$ is displayed in Figs. 2(b) and 2(c) (right-hand scale), respectively, and the reciprocal susceptibility of both compounds shows the Curie–Weiss-type behavior in the PM region. The average values of the effective magnetic moments for $(Ho_{0.75}Y_{0.25})_5Pd_2$ and $(Ho_{0.5}Y_{0.5})_5Pd_2$ are determined to be 10.3 μ_B/RE and 7.5 μ_B/RE, respectively, and the corresponding values of the paramagnetic Curie temperature θ_p are obtained to be 30 K and 22 K. As the yttrium content increases, both the effective magnetic moments and paramagnetic Curie temperatures of the $(Ho_{1-x}Y_x)_5Pd_2$ compounds show a decrease trend, however, not linearly. To investigate the thermal hysteresis near the T_g, the $(Ho_{1-x}Y_x)_5Pd_2$ ($x = 0$, 0.25, and 0.5) samples were first subjected to an applied field of 200 Oe and measured on cooling and then heating models. The obtained M–T curves for $(Ho_{1-x}Y_x)_5Pd_2$ ($x = 0$, 0.25, and 0.5) are shown in Figs. 3(a)–3(c), respectively. For both Ho_5Pd_2 and $(Ho_{0.75}Y_{0.25})_5Pd_2$, the maximum thermal hysteresis is approximately 1.7 K, whereas that for the $(Ho_{0.5}Y_{0.5})_5Pd_2$ compound is determined to be less than 1 K, indicating that the substitution of Y for Ho can reduce the thermal hysteresis of $(Ho_{1-x}Y_x)_5Pd_2$. The relatively small values of thermal hysteresis suggest that the phase transitions in these compounds probably belong to the SOT type, which is beneficial for the efficiency of the magnetic refrigeration.

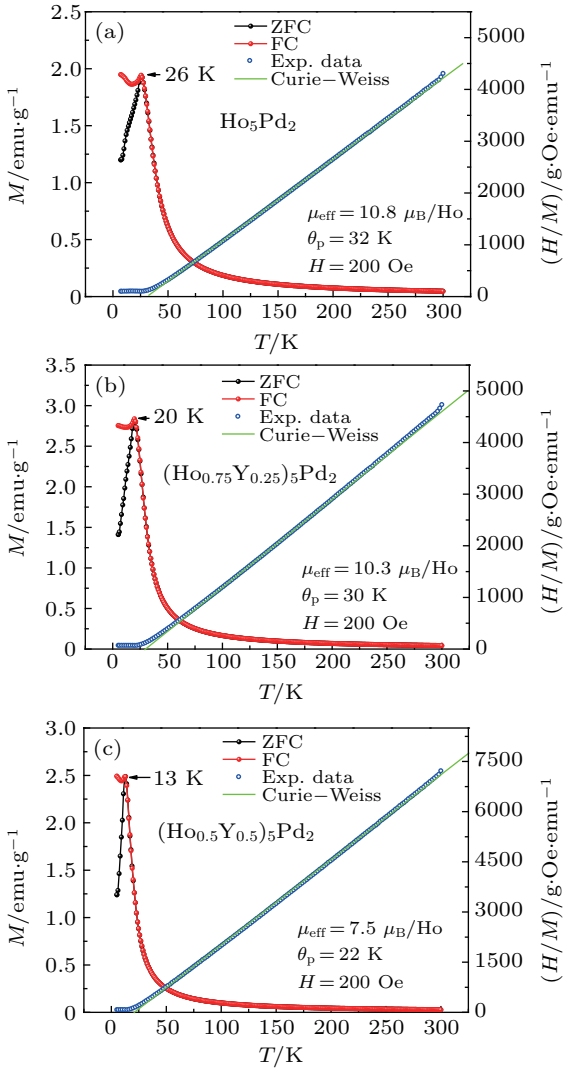


Fig. 2. Temperature dependence of ZFC and FC magnetizations (left scale) and the reciprocal susceptibility ($1/\chi = H/M$, right scale) along with the Curie–Weiss fit for (a) Ho_5Pd_2, (b) $(Ho_{0.75}Y_{0.25})_5Pd_2$, and (c) $(Ho_{0.5}Y_{0.5})_5Pd_2$ under the magnetic field of 200 Oe.

To evaluate the MCEs for the series of $(Ho_{1-x}Y_x)_5Pd_2$ ($x = 0$, 0.25, and 0.5), sets of isothermal magnetization curves at different temperature steps in magnetic fields up to 5 T were recorded, as displayed in Figs. 4(a), 4(c), and 4(e). After one isothermal curve was recorded, the applied field was

isothermally reduced to zero, and then the temperature was increased slowly for another curve. It can be observed that there is a considerable difference among the *M*–*H* for each compound in different temperature ranges. In the magnetic isotherms below T_g, the magnetizations increase rapidly with the increase of the magnetic field, showing the feature of the ferromagnetism, which suggests that the FM exchange interaction dominates in the spin-glass state of the $(Ho_{1-x}Y_x)_5Pd_2$ ($x = 0$, 0.25, and 0.5) compounds. It is also observed that the magnetization does not saturate under field as high as 5 T and the similar kind of *M*–*H* curves with non-saturating behavior was observed in the compounds showing glassy magnetic behavior and also in canted AFM systems.[57,59] In the PM region, there exist curvatures in the isothermal curves near T_g, probably indicating the existence of short-range FM correlations in the PM state which are also induced by the applied field, and the *M*–*H* curves become more and more linear with the temperature increasing. This phenomenon comes from the competition of the applied field and temperature for the FM state. By comparing the *M*–*H* curves of Ho_5Pd_2,

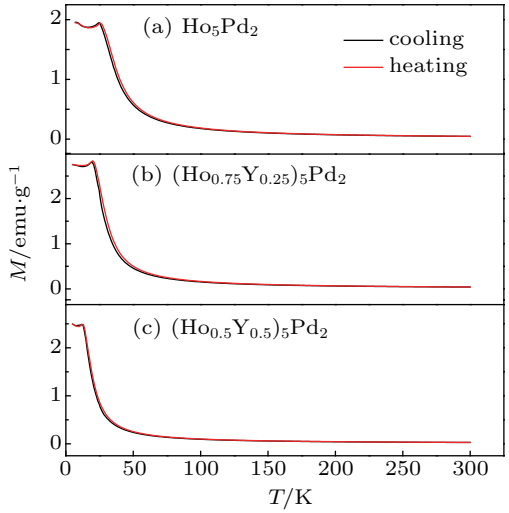


Fig. 3. The *M*–*T* curves under a magnetic field of 200 Oe on heating and cooling processes for (a) Ho_5Pd_2, (b) $(Ho_{0.75}Y_{0.25})_5Pd_2$, and (c) $(Ho_{0.5}Y_{0.5})_5Pd_2$.

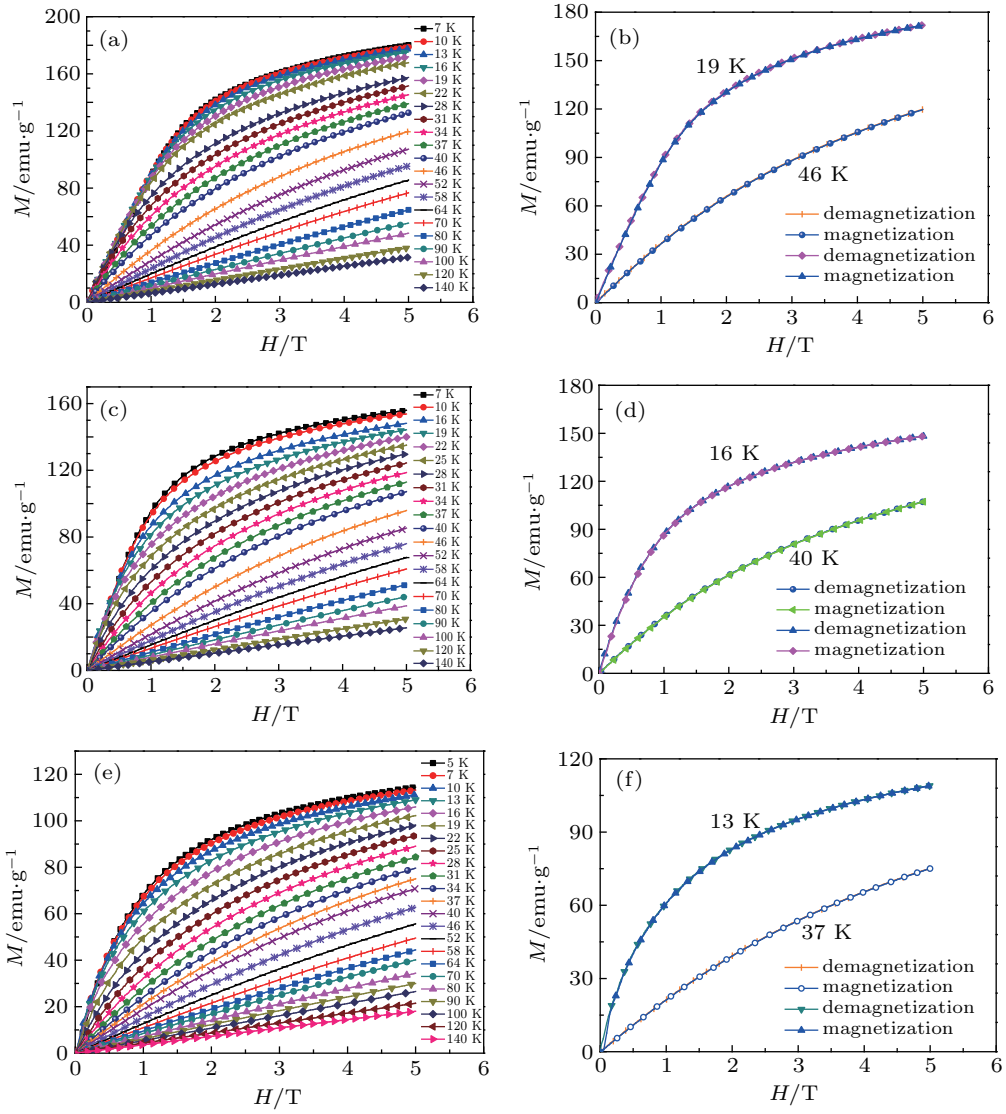


Fig. 4. The isothermal magnetization curves for (a) Ho_5Pd_2, (c) $(Ho_{0.75}Y_{0.25})_5Pd_2$, and (e) $(Ho_{0.5}Y_{0.5})_5Pd_2$ measured with the magnetizing process up to 5 T. The magnetization and demagnetization curves for (b) Ho_5Pd_2, (d) $(Ho_{0.75}Y_{0.25})_5Pd_2$, and (f) $(Ho_{0.5}Y_{0.5})_5Pd_2$.

$(Ho_{0.75}Y_{0.25})_5Pd_2$, and $(Ho_{0.5}Y_{0.5})_5Pd_2$, it is found that the magnetizations decrease obviously with increasing yttrium content, which happens because the Y element is nonmagnetic. To examine the magnetic hysteresis in $(Ho_{1-x}Y_x)_5Pd_2$ ($x = 0$, 0.25, and 0.5), two selected magnetization isotherms for each compound on increasing and decreasing fields near T_g were measured and are shown in Figs. 4(b), 4(d), and 4(f), respectively. It is clearly seen that the isothermal curves in the magnetizing process are perfectly overlapping with those in the demagnetizing process, exhibiting no magnetic hysteresis and a perfect reversibility of the magnetic phase transitions, which is the characteristic of the SOT.

It is well-known that a large magnetic entropy change is expected around the magnetic transition temperature since the magnetization changes rapidly by varying the temperature and the MCE has a strong correlation with the order of the corresponding magnetic phase transition. Thus, it is important to understand the nature of magnetic transition in $(Ho_{1-x}Y_x)_5Pd_2$. In general, Arrott plots are used to determine the type (FOT or SOT) of the phase transition of a compound. According to the Banerjee criterion,[60] the nature of the magnetic transition is of the second order if all the Arrott plots have a positive slope. Meanwhile, if some of the curves display a negative slope or inflection at some points, the nature of the magnetic transition is of the first order. To further understand the nature of the magnetic transition in the $(Ho_{1-x}Y_x)_5Pd_2$ ($x = 0$, 0.25, and 0.5) compounds, the measured M–H isotherms for the compounds at various temperatures were converted to the M^2 vs. H/M plots (Arrott plots) as presented in Figs. 5(a), 5(c), and 5(e), respectively. Neither negative slope nor inflection can be observed in the Arrott plots near T_g in each sample, which shows the occurrence of the second order magnetic phase transition from spin-glass state to PM state for the Ho_5Pd_2, $(Ho_{0.75}Y_{0.25})_5Pd_2$, and $(Ho_{0.5}Y_{0.5})_5Pd_2$ compounds.

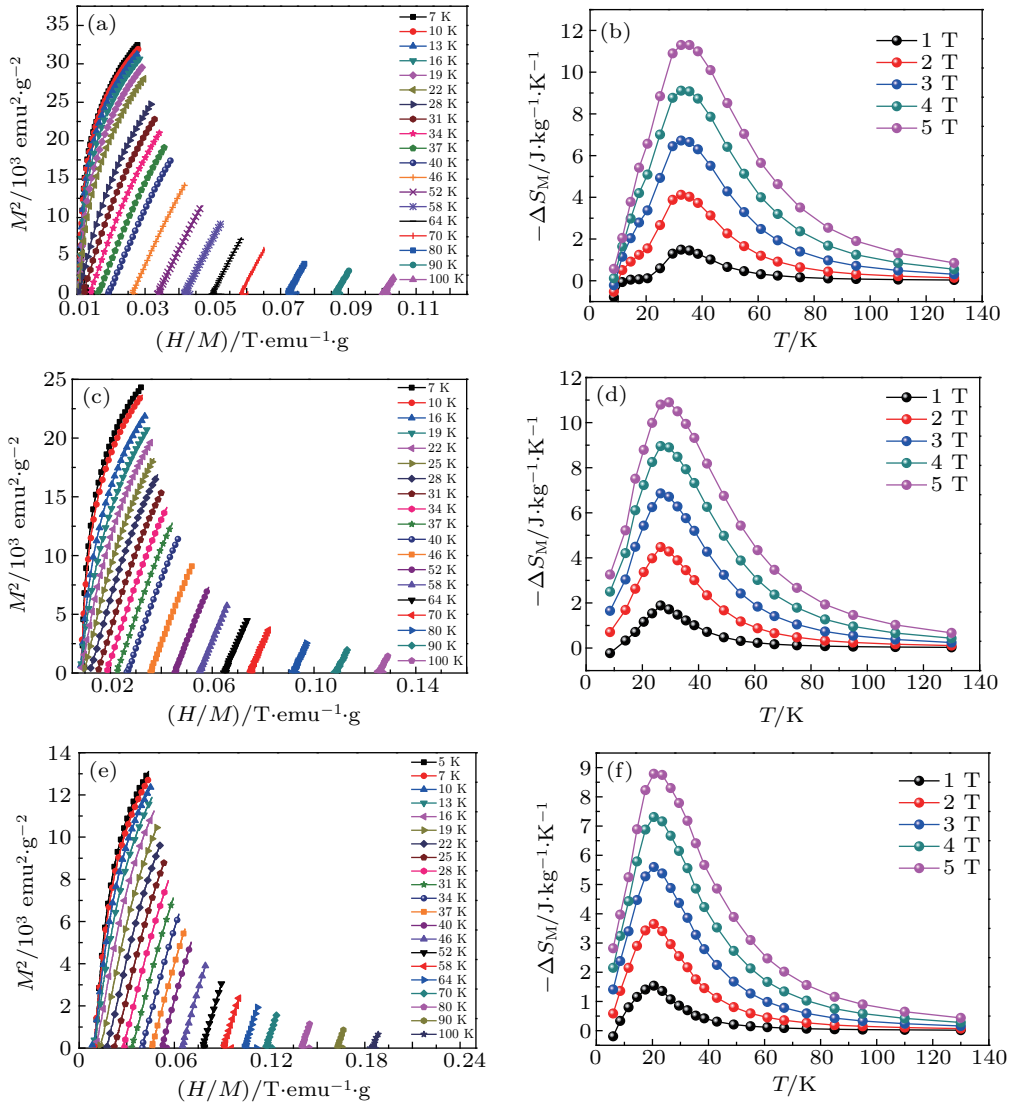


Fig. 5. The plots of H/M versus M^2 (Arrott curve) for (a) Ho_5Pd_2, (c) $(Ho_{0.75}Y_{0.25})_5Pd_2$, and (e) $(Ho_{0.5}Y_{0.5})_5Pd_2$ at different temperatures. The isothermal magnetization curves measured with the magnetizing process up to 5 T. The magnetic entropy change $-\Delta S_M$ as a function of temperature for various magnetic field changes for (b) Ho_5Pd_2, (d) $(Ho_{0.75}Y_{0.25})_5Pd_2$, and (f) $(Ho_{0.5}Y_{0.5})_5Pd_2$.

The temperature dependence of ΔS_M for $(Ho_{1-x}Y_x)_5Pd_2$ ($x = 0$, 0.25, and 0.5) under a magnetic field change of 5 T was derived from the isothermal M–H curves by utilizing the Maxwell relation $\Delta S_M(T,H) = \int_0^H (\frac{\partial M}{\partial T})_H dH$, where T is the absolute temperature and H is the applied magnetic field, and is shown in Figs. 5(b), 5(d), and 5(f), respectively. As expected, the maximum values of the entropy change ΔS_M occur near the transition temperatures and increase with the increase of the magnetic field. The peaks of ΔS_M for $(Ho_{1-x}Y_x)_5Pd_2$ shift to the lower temperature with the increase of Y content, indicating that the Y doping can decrease the working temperature range for the series of $(Ho_{1-x}Y_x)_5Pd_2$ compounds. Here, it should be noted that the ΔS_M–T curve for Ho_5Pd_2 has another peak which is obvious under the low magnetic field change. This is probably due to that there exits another magnetic transition in the sample Ho_5Pd_2 below the T_g, which is likely the spin-reorientation. For the samples $(Ho_{0.75}Y_{0.25})_5Pd_2$ and $(Ho_{0.5}Y_{0.5})_5Pd_2$, there are also inflections in the ΔS_M–T curves below the temperatures of T_g, however, inconspicuously. Under the magnetic field changes of 0–5 T, the maximum values of the magnetic entropy change ($-\Delta S_M$) for Ho_5Pd_2, $(Ho_{0.75}Y_{0.25})_5Pd_2$, and $(Ho_{0.5}Y_{0.5})_5Pd_2$ are evaluated to be 11.5 J·kg^{-1}·K^{-1}, 11.1 J·kg^{-1}·K^{-1}, and 8.9 J·kg^{-1}·K^{-1}, respectively.

As mentioned previously, the refrigerant capacity (RC) is also an important criterion of a potential magnetic refrigerant. Based on the ΔS_M–T curves, the RC is estimated using the approach suggested by Gschneidner *et al.*[1] and defined as RC $= \int_{T_1}^{T_2} |\Delta S_M| dT$, where T_1 and T_2 are the temperatures corresponding to the half-maximum values at the two sides of the ΔS_M peak, respectively. The RC values for the Ho_5Pd_2, $(Ho_{0.75}Y_{0.25})_5Pd_2$, and $(Ho_{0.5}Y_{0.5})_5Pd_2$ compounds are determined to be 382.3 J·kg^{-1}, 336.2 J·kg^{-1}, and 242.5 J·kg^{-1} for a field change of 0–5 T, respectively. The considerable RC values suggest that the $(Ho_{1-x}Y_x)_5Pd_2$ compounds could be the attractive candidate materials for the magnetic refrigerator working at low temperature. The transition temperature (T_{tr}), the values of ($-\Delta S_M$), RC as well as the lattice parameters for the $(Ho_{1-x}Y_x)_5Pd_2$ compounds are summarized in Table 1.

Table 1. The lattice parameters, the transition temperature (T_g), the maximum entropy change $-\Delta S_M$, as well as the refrigerant capacity under $\Delta H = 5$ T for $(Ho_{1-x}Y_x)_5Pd_2$ ($x = 0$, 0.25, and 0.5).

Compounds	Lattice parameters		T_g/K	$\lvert\Delta S_M\rvert$/J·kg^{-1}·K^{-1}	RC/J·kg^{-1}
	a/Å	V/Å^3			
Ho_5Pd_2	13.4428	2429.2	26	11.5	382.3
$(Ho_{0.75}Y0_{.25})_5Pd_2$	13.4906	2455.2	20	11.1	336.2
$(Ho_{0.5}Y_{0.5})_5Pd_2$	13.5315	2477.7	13	8.9	114.8

4. Conclusion

In the present work, the crystal structure, magnetic transitions, and magnetocaloric properties of the $(Ho_{1-x}Y_x)_5Pd_2$ ($x = 0$, 0.25, and 0.5) compounds were investigated experimentally by XRD and magnetic measurements. All the compounds crystallize in a cubic Dy_5Pd_2-type with the space group $Fd3m$, and the lattice parameter a and unit-cell volume V for $x = 0$, 0.25, and 0.5 were determined to be 13.4428 Å, 2429.2 Å^3, 13.4906 Å, 2455.2 Å^3; and 13.5315 Å, 2477.7 Å^3, respectively. A second order spin-glass to PM transition occurs in each sample and the transition temperatures (T_g) were determined to be 26 K, 20 K, and 13 K for $x = 0$, 0.25, and 0.5, respectively. In the PM region, the reciprocal susceptibilities for all the compounds obey the Curie–Weiss law. The paramagnetic Curie temperature (θ_p) for Ho_5Pd_2, $(Ho_{0.75}Y_{0.25})_5Pd_2$, and $(Ho_{0.5}Y_{0.5})_5Pd_2$ were determined to be 32 K, 30 K, and 22 K, and the corresponding effective magnetic moments (μ_{eff}) were determined to be 10.8 μ_B/Ho, 10.3 μ_B/RE, and 7.5 μ_B/RE, respectively. Using the Maxwell relation, the magnetic entropy changes of the $(Ho_{1-x}Y_x)_5Pd_2$ ($x = 0$, 0.25, and 0.5) compounds were calculated. For a field change of 5 T, the maximum magnetic entropy changes of the Ho_5Pd_2, $(Ho_{0.75}Y_{0.25})_5Pd_2$, and $(Ho_{0.5}Y_{0.5})_5Pd_2$ compounds are 11.5 J·kg^{-1}·K^{-1}, 11.1 J·kg^{-1}·K^{-1}, and 8.9 J·kg^{-1}·K^{-1}, respectively, with the corresponding RC values of 382.3 J·kg^{-1}, 336.2 J·kg^{-1}, and 242.5 J·kg^{-1}. The considerable MCE values and adjustable working temperature range indicate that the $(Ho_{1-x}Y_x)_5Pd_2$ compounds could be promising candidates for magnetic refrigeration at low temperatures.

References

[1] Gschneidner Jr K A, Pecharsky V K and Tsokol A O 2005 *Rep. Prog. Phys.* **68** 1479
[2] Shen B G, Sun J R, Hu F X, Zhang H W and Cheng Z H 2009 *Adv. Mater.* **21** 4545
[3] Brück E 2005 *J. Phys. D: Appl. Phys.* **38** R381
[4] de Oliveira N A and Von Ranke P J 2010 *Phys. Rep.* **489** 89
[5] Pecharsky V K and Gschneidner Jr K A 1999 *J. Magn. Magn. Mater.* **200** 44
[6] Pecharsky V K and Gschneidner Jr K A 2001 *J. Appl. Phys.* **90** 4614
[7] Provenzano V, Shapiro A J and Shull R D 2004 *Nature* **429** 853
[8] Shen J, Gao B, Zhang H W, Hu F X, Li Y X, Sun J R and Shen B G 2007 *Appl. Phys. Lett.* **91** 142504
[9] Pecharsky V K and Gschneidner Jr K A 1997 *Phys. Rev. Lett.* **78** 4494
[10] Gschneidner Jr K A 2009 *Acta Mater.* **57** 18
[11] Hu F X, Shen B G, Sun J R, Cheng Z H, Rao G H and Zhang X X 2001 *Appl. Phys. Lett.* **78** 3675
[12] Hu F X, Shen B G, Sun J R and Zhang X X 2000 *Chin. Phys.* **9** 0550
[13] Zhang X X, Wen G H, Wang F W, Wang W H, Yu C H and Wu G H 2000 *Appl. Phys. Lett.* **77** 3072

[14] Zhang X X, Wang F W and Wen G H 2001 *J. Phys.: Condens. Matter* **13** L747
[15] Tegus O, Brück E, Buschow K H J and De Boer F R 2002 *Nature* **415** 150
[16] Wada H and Tanabe Y 2001 *Appl. Phys. Lett.* **79** 3302
[17] Hu F X, Shen B G, Sun J R and Wu G H 2001 *Phys. Rev. B* **64** 132412
[18] Krenke T, Duman E, Acet M, Wassermann E F, Moya X, Mañosa L and Planes A 2005 *Nat. Mater.* **4** 450
[19] Kainuma R, Imano Y, Ito W, Sutou Y, Morito H, Okamoto S, Kitakami O, Oikawa K, Fujita A, Kanomata T and Ishida K 2006 *Nature* **439** 957
[20] Planes A, Mañosa L and Acet M 2009 *J. Phys.: Condens. Matter* **21** 233201
[21] Liu J, Gottschall T, Skokov K P, Moore J D and Gutfleisch O 2012 *Nat. Mater.* **11** 620
[22] Tishin A M, Spichkin Y I, in: Coey J M D, Tilley D R and Vij D R 2003 *The Magnetocaloric Effect and its Applications* (Bristol: Institute of Physics Publishing)
[23] Wada H, Tanabe Y, Shiga M, Sugawara H and Sato H 2001 *J. Alloys Compd.* **316** 245
[24] Li L W, Yi Y L, Su K P, Qi Y, Huo D X and Pöttgen R 2016 *J. Mater. Sci.* **51** 5421
[25] Huo J J, Du Y S, Cheng G, Wu X F, Ma L, Wang J, Xia Z C and Rao G H 2018 *J. Rare Earth* **36** 1044
[26] Chen J, Shen B G, Dong Q Y and Sun J R 2010 *Solid State Commun.* **150** 157
[27] Wang L C and Shen B G 2014 *Rare Met.* **33** 239
[28] Chen J, Shen B G, Dong Q Y and Sun J R 2010 *Solid State Commun.* **150** 1429
[29] Singh N K, Kumar P, Mao Z, Paudyal D, Neu V, Suresh K G, Pecharsky V K and Gschneidner K A 2009 *J. Phys.: Condens. Matter* **21** 456004
[30] Mo Z J, Shen J, Gao X Q, Liu Y, Wu J F, Shen B G and Sun J R 2015 *Chin. Phys. B* **24** 037503
[31] Zheng X Q, Shen J, Hu F X, Sun J R and Shen B G 2016 *Acta Phys. Sin.* **65** 217502 (in Chinese)
[32] Mo Z J, Sun Q L, Wang C H, Wu H Z, Li L, Meng F B, Tang C C, Zhao Y and Shen J 2017 *Ceram. Int.* **43** 2083
[33] Wang Y X, Zhang H, Wu M L, Tao K, Li Y W, Yan T, Long K W, Long T, Pang Z and Long Y 2016 *Chin. Phys. B* **25** 127104
[34] Zhang H, Shen B G, Xu Z Y, Shen J, Hu F X, Sun J R and Long Y 2013 *Appl. Phys. Lett.* **102** 092401
[35] Zhang H, Sun Y J, Yang L H, Niu E, Wang H S, Hu F X, Sun J R and Shen B G 2014 *J. Appl. Phys.* **115** 063901
[36] Wu M L, Zhang H, Xu Z Y, Wang Y X, Tao K, Zhang Y L, Yan T, Long K W, Li Y W, Shen J Y and Long Y 2017 *Intermetallics* **83** 38
[37] Wang Y X, Zhang H, Long K W, Xing C F, Xiao Y N, Su L Q, Wang L C and Long Y 2018 *Intermetallics* **100** 175
[38] Mo Z J, Hao Z H, Shen J, Li L, Wu J F, Hu F X, Sun J R and Shen B G 2015 *J. Alloys Compd.* **649** 674
[39] Li L W, Xu C, Yuan Y and Zhou S Q 2018 *Mater. Res. Lett.* **6** 413
[40] Wu M L, Zhang H, Long K W, Tao K, Wang Y X, Xing C F, Xiao Y N, Wang L C and Long Y 2017 *Mater. Lett.* **205** 40
[41] Zheng X Q and Shen B G 2017 *Chin. Phys. B* **26** 027501
[42] Li Y W, Zhang H, Yan T, Long K W, Wang H S, Xue Y J, Cheng C and Zhou H B 2015 *J. Alloys Compd.* **651** 278
[43] Mo Z J, Shen J, Gao X Q, Liu Y, Tang C C, Wu J F, Hu F X, Sun J R and Shen B G 2015 *J. Alloys Compd.* **626** 145
[44] Li L W, Hu G H, Qi Y and Umehara I 2017 *Sci. Rep.* **7** 42908
[45] Mo Z J, Shen J, Yan L Q, Wu J F, Wang L C, Lin J, Tang C C and Shen B G 2013 *Appl. Phys. Lett.* **102** 192407
[46] Mo Z J, Shen J, Yan L Q, Tang C C, Lin J, Wu J F, Sun J R, Wang L C, Zheng X Q and Shen B G 2013 *Appl. Phys. Lett.* **103** 052409
[47] Berkowitz A E, Holtzberg F and Methfessel S 1964 *J. Appl. Phys.* **35** 1030
[48] Loebich O and Raub J R E 1973 *J. Less Common Met.* **30** 47
[49] Fornasini M L and Palenzona A 1974 *J. Less Common Met.* **38** 77
[50] Yakinthos J K, Anagnostopoulos T and Ikonomou P F 1977 *J. Less Common Met.* **51** 113
[51] Klimczak M, Talik E, Winiarski A and Troć R 2006 *J. Alloys Compd.* **423** 62
[52] Sharma M K, Yadav K and Mukherjee K 2018 *J. Phys.: Condens. Matter* **30** 215803
[53] Paramanik T, Samanta T, Ranganathna R and Das I 2015 *RSC Adv.* **5** 47860
[54] Gubkin A F, A Sherstobitova E, Terentyev P B, Hoser A and Baranov N V 2013 *J. Phys.: Condens. Matter* **25** 236003
[55] Samanta T, Das I and Banerjee S 2007 *Appl. Phys. Lett.* **91** 082511
[56] Toyoizumi S, Kitazawa H, Kawamura Y, Mamiya H, Terada N, Tamura R, Dönni A, Morita K and Tamaki A 2015 *J. Appl. Phys.* **117** 17D101
[57] Mydosh J A 1993 *Spin Glasses: an Experimental Introduction* (London: Taylor and Francis)
[58] Sh, P M, Meyer A L, Streicher M, Wilson A, Rash T, Roth M W, Kidd T E and Strauss L H 2012 *Phys. Rev. B* **85** 144432
[59] McDannald A, Kuna L, Jain M 2013 *J. Appl. Phys.* **114** 113904
[60] Banerjee B K 1964 *Phys. Lett.* **12** 16